Pore-scale modeling of saturated permeabilities in random sphere packings

Chongxun Pan, Markus Hilpert, and Cass T. Miller
Department of Environmental Science and Engineering, University of North Carolina at Chapel Hill, Chapel Hill, North Carolina 27599-7400
(Received 22 March 2001; published 20 November 2001)

We use two pore-scale approaches, lattice-Boltzmann (LB) and pore-network modeling, to simulate single-phase flow in simulated sphere packings that vary in porosity and sphere-size distribution. For both modeling approaches, we determine the size of the representative elementary volume with respect to the permeability. Permeabilities obtained by LB modeling agree well with Rumpf and Gupte's experiments in sphere packings for small Reynolds numbers. The LB simulations agree well with the empirical Ergun equation for intermediate but not for small Reynolds numbers. We suggest a modified form of Ergun's equation to describe both low and intermediate Reynolds number flows. The pore-network simulations agree well with predictions from the effective-medium approximation but underestimate the permeability due to the simplified representation of the porous media. Based on LB simulations in packings with log-normal sphere-size distributions, we suggest a permeability relation with respect to the porosity, as well as the mean and standard deviation of the sphere diameter.

DOI: 10.1103/PhysRevE.64.066702 PACS number(s): 02.70.−c, 47.55.Mh, 47.15.Gf

I. INTRODUCTION

Pore-scale models improve our understanding of flow and transport phenomena in porous media but can also be used to obtain macroscale constitutive relationships, which are necessary to close continuum theories for these phenomena [1]. Using pore-scale models as quantitative predictive tools, however, is not straightforward because the numerical domains are limited in size by finite computational resources, a microscopic description of the pore-space geometry is needed, and the numerical pore-scale model needs to be parametrized. This paper deals with the prediction of single-phase flow using lattice-Boltzmann (LB) and pore-network models. Faithful modeling of single-phase flow is, for example, important for species transport models, the predictive capabilities of which require an accurate velocity field.

On the macroscale, single-phase flow in porous media at low Reynolds numbers is described by Darcy's law—or to be more accurate, by its generalization to three-dimensional flow in isotropic media [2]:

$$u_d = -\frac{\kappa}{\eta}(\nabla p + \rho g \nabla z), \tag{1.1}$$

where u_d is the Darcy velocity or the specific discharge, κ the saturated permeability, η the dynamic viscosity, p the fluid pressure, g the gravitational acceleration, and z the vertical coordinate. Because of the complicated geometry of natural pore spaces, analytical forms for the constitutive relation κ are not available. A great deal of effort has been devoted to empirical relationships among κ and porous medium properties. The Carman-Kozeny [3] is a widely used relationship, which gives κ for granular media consisting of arbitrarily shaped particles:

$$\kappa_{\mathrm{CK}} = \frac{\overline{D_2}^2}{180}\frac{\phi^3}{(1-\phi)^2}, \tag{1.2}$$

where

$$\overline{D_2} = \frac{\int D^3 N(D) dD}{\int D^2 N(D) dD} \tag{1.3}$$

is the surface average diameter, ϕ the porosity, and $N(D)$ the distribution function of the grain diameter D. The Blake-Kozeny relation [4] has the same form as the Carman-Kozeny, but the constant differs by as much as 20%. Rumpf and Gupte [5] measured κ in random sphere packings and obtained the empirical relation

$$\kappa_{\mathrm{RG}} = \frac{\overline{D_2}^2}{5.6}\phi^{5.5}. \tag{1.4}$$

These relations' shortcomings include (1) the limited accuracy of the Carman-Kozeny relation in predicting κ for the special case of sphere packings, (2) the breakdown of the Carman-Kozeny relation for low and high porosities [6,7], and (3) the lack of broad experimental support for the Rumpf-Gupte relation.

Darcy's law loses its validity if Re exceeds a critical value Re_0 that ranges between 0.1 and 75, depending on the pore structure and the definition of Re_0 [8]. As Re increases, there is a transition from creeping flow to another laminar flow regime, where inertial forces become important [9]. Many correlations describing flow for $\mathrm{Re} > \mathrm{Re}_0$ have been presented in the literature. The best known relationship is Ergun's equation, which was obtained in uniformly packed columns for intermediate values of Re. It can be formulated as

$$\frac{\nabla p}{\eta u_d}\frac{\overline{D_2}^2\phi^3}{(1-\phi)^2} = A + B\frac{\mathrm{Re}}{1-\phi}, \tag{1.5}$$

where $A = 150$ and $B = 1.75$ [2]. MacDonald *et al.* [10] suggested $A = 180$ and B to lie between 1.8 and 4.0 in order to

match data from a variety of porous media. After our knowledge, a correlation describing flow both in the Darcian ($Re < Re_0$) and non-Darcian ($Re > Re_0$) regime has not been presented yet.

Pore-network [1] and LB modeling [11] are considered useful for simulating flow phenomena in porous media. LB methods simulate flow by describing the movement and collisions of quasiparticles along a lattice. LB models have been used to investigate various aspects of single-phase flow in porous media, including flow through sphere packings [12,13], cemented media [14], and media with randomly placed identical obstacles [15], critical porosities [6], the representative elementary volume (REV) for permeability [16,17], and higher Reynolds number flow [18]. But thorough investigations on the REV's, as well as a comparison between simulations and existing permeability relationships, have not yet been presented for a broad range of sphere packings.

Pore-network models are simplified representations of porous media that usually consist of analogs of pore bodies and throats, along with a description of how the pore bodies are connected via the pore throats. The main difficulty in using pore-network models in a quantitative predictive sense lies in choosing the geometric shape, sizes, locations, and orientations of the pore bodies and throats. Quantitative predictions for κ require a calibration of the network geometry, which can be accomplished by estimating the pore sizes from measured capillary pressure-saturation curves [19,20], deriving the network from a detailed representation of a sphere packing, using a subdivision of the packing into tetrahedra [21], mapping a three-dimensional digital representation of the pore space onto the statistical properties of a pore network [22,23], or identifying the actual positions and sizes of pore bodies and throats from a three-dimensional digital representation [24]. Although methods for estimating pore sizes from grain-size data exist [25,26], an approach that predicts κ from a network model, based only on grain-size data and porosity, has not been presented [1].

The objectives of this work are (1) to implement and evaluate an LB and a pore-network model to simulate flow through sphere packings, (2) to find a statistically supported REV for packings with varying uniformity, using both models, (3) to investigate the transition region between Darcian and non-Darcian flow, (4) to compare LB simulations with existing empirical relations for permeability for a broad range of packings, and (5) to formulate a correlation function for the permeability in sphere packing with log-normal sphere-size distribution.

II. NUMERICAL METHODS

A. Porous media

Modeling flow in porous media requires detailed information about the pore structure, which necessitates either small-scale experimental measurements using, for example, nuclear magnetic resonance (NMR) or serial sections, or a theoretical approach to provide a meaningful representation. The experimental measurements, however, are time-consuming and expensive, so the use of simulated porous media is conceptually appealing. Yang, Miller, and Turcoliver [27] developed a theoretical approach for packing a large number of random-size nonoverlapping spheres. We use log-normal sphere-size distributions, because many natural porous media can be described by such a distribution [9]. The simulated porous media are generated by using easily quantifiable macroscopic measures of a porous medium as input parameters: the mean $\overline{D}$ and standard deviation σ_D of the sphere diameter D, and the porosity ϕ as well.

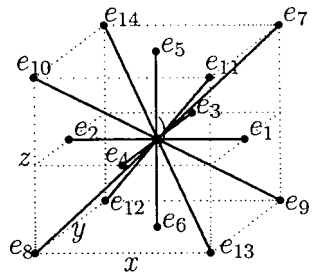

FIG. 1. Lattice structure of the LB model with 15 velocity directions per lattice node.

B. Lattice-Boltzmann simulation

1. Model structure

We implemented a three-dimensional LB model as described in the literature [28,29]. This model has 15 fixed velocity vectors $\vec{e}_i$, where $i=1,2,\ldots,15$, and includes a rest particle ($i=15$). Figure 1 shows the lattice structure. The distribution function $f_i(\vec{x},t)$ stands for the probability of finding a particle with velocity $\vec{e}_i$ at location $\vec{x}$ and time t. The fluid density is given by $\rho' = \Sigma_i f_i$ and the velocity by $\vec{u}' = \Sigma_i f_i \vec{e}_i / \rho'$. Evolution in time is ruled by

$$f_i(\vec{x}+\vec{e}_i, t+1) - f_i(\vec{x},t) = \frac{1}{\tau}[f_i^{(eq)}(\vec{x},t) - f_i(\vec{x},t)]. \tag{2.1}$$

The left-hand side of this equation represents the interaction-free movement of the particles. Particle collisions are described on the right-hand side, with the approximation of a single-rate relaxation to the equilibrium distribution function $f_i^{(eq)}$, which depends locally on $\vec{u}'$ and ρ'. If this function is chosen properly, Eq. (2.1) is equivalent to a nondimensional Navier-Stokes equation $d\vec{u}'/dt = -(1/\rho')\vec{\nabla}p' + \nu'\vec{\nabla}^2\vec{u}'$ in the limit of incompressible flow, where the kinematic viscosity is given by $\nu' = (2\tau - 1)/6$ and the pressure by $p' = 3\rho'/8$ [28,30].

The no-slip boundary condition at the solid surface is implemented by a bounce-back scheme $f_j(\vec{x},t+1) - f_i(\vec{x},t) = 1/\tau[f_i^{(eq)}(\vec{x},t) - f_i(\vec{x},t)]$, where j is related to i by $\vec{e}_j = -\vec{e}_i$ [29]. This scheme assumes the wall with the no-slip boundary condition to be located midway between the solid node and the fluid node, where the particle originates. At the inlet and outlet, we prescribe constant densities ρ_1' and ρ_2' by implementing the pressure boundary conditions as described in Refs. [28,30].

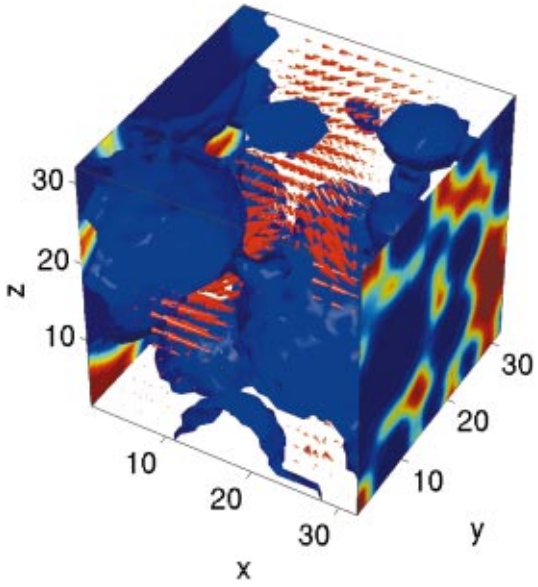

FIG. 2. (Color) Porous medium with velocity field obtained by LB modeling. Blue: solid phase. The size of the red cone indicates the magnitude of the fluid velocity.

One can determine important macroscopic measures of the flow field from the microscopic nondimensional variables. The permeability is $\kappa = 8\nu' L^2 \rho' u_d' / (3N\Delta\rho')$, where L is the length along the flow direction, N the number of lattice nodes along the flow direction, u_d' the nondimensional Darcy velocity, and $\Delta\rho' = \rho_1' - \rho_2'$. The Reynolds number is $\mathrm{Re} = u_d' \overline{D_2} N / (\nu' L)$. Figure 2 demonstrates part of a digital porous medium with the steady-state flow velocity field $\vec{u}'$ obtained by a LB simulation.

2. Validation of an LB model

To validate our LB code, we simulated steady-state laminar flow in a duct with a square cross section. If $|\Sigma_{\vec{x}} |u'(\vec{x},t)| / \Sigma_{\vec{x}} |u'(\vec{x},t+50)| - 1| \leqslant 10^{-6}$; we considered the simulation converged. We studied convergence with respect to the relaxation time τ and the duct width m measured in lattice units. We achieved second-order convergence as described elsewhere [28,30,29]. For $\tau = 1$, the relative error between the simulated and analytical velocity in the duct center (where u' is maximum) decreased from 39% for $m = 3$ to 1% for $m = 17$, consistent with the investigation of Maier *et al.* [29]. For $\tau = 0.8$, which usually requires more time steps to achieve convergence, we obtained 11% relative error for $m = 3$ and 0.5% for $m = 17$. Therefore, we used $\tau = 0.8$ for all remaining simulations. Zou and He [28] presented a more complete investigation on the impact of τ. Our results show that, with sufficient spatial resolution, a LB model accurately simulates flow processes.

C. Pore-network modeling

1. Model structure

Our pore-network model consists of cubic pore bodies connected by pore throats with square cross sections. Each pore body is connected to at most six neighboring bodies via pore throats along the lattice axes; the maximum coordination number is $Z_0 = 6$. We obtained coordination numbers $Z < 6$ by cutting the pore throats randomly. The network is periodic in both horizontal directions. The top and bottom of the network are connected to constant pressure reservoirs.

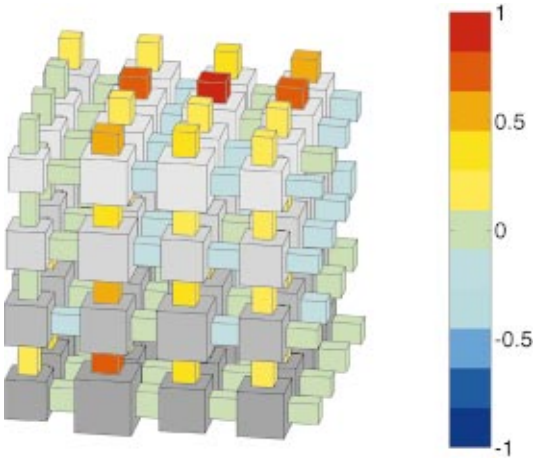

FIG. 3. (Color) Simulation of a single-phase flow in a pore network. The shading of the pores stands for the pressure, which decreases from the bottom to the top of the network. The colors of the throats show the normalized flow rates.

Incompressible single-phase flow of a viscous fluid is modeled as described by Fenwick and Blunt [31]. The pressure drop between the two adjacent bodies i and j is $p_i - p_j = Q_{ij} / g_{ij}$, where Q_{ij} is the flow rate and g_{ij} the conductance between pore bodies i and j. g_{ij} depends on the local network geometry and the dynamic viscosity η. Note that pressure drops occur in both pore throats and bodies.

Applying the continuity equation $\Sigma_j Q_{ij} = 0$, at all pore bodies except those on both flow boundaries where pressures are fixed, yields a sparse symmetric system of linear equations. The unknown pressures are determined using the iterative conjugate gradient method. We compute the total flow rate through the network and determine κ using Eq. (1.1). Figure 3 illustrates a flow simulation in a pore network.

2. Pore-network calibration

For calibrating the pore networks, we mapped the digital pore space onto the size distributions of the pore bodies and throats and onto the coordination number Z of the network. We first determined integral geometric quantities of the sphere packings, the morphological pore-size distribution and the genus, and used these data to calibrate the network. The calibration approach is described in detail in Hilpert, Glantz, and Miller [32], who used it to obtain good predictions for hysteretic capillary pressure-saturation curves. We will only briefly describe its methodology.

The cumulative morphological pore-size distribution

$$F(r) = \frac{\mathrm{Vol}[\cup (S_{\vec{x}}(r) : S_{\vec{x}}(r) \subset P)]}{\mathrm{Vol}[P]} \qquad (2.2)$$

quantifies that fraction of the pore space P that is at least as large as a sphere S of radius r. The subscript $\vec{x}$ denotes the translation of S by the vector $\vec{x}$. $F(r)$ can be readily obtained for digital porous media [33]. A measure for the connectivity of a three-dimensional geometric object is the Euler-Poincaré characteristic χ [34]. For sphere packings subject to gravity, χ of the pore space P is

$$\chi(P)=1-G(P), \tag{2.3}$$

where the genus G is the maximum number of fully penetrating cuts that one can make through P without producing more separate components. χ can be readily obtained for digital pore spaces by counting the corners, edges, surfaces, and cubes of P [35].

We make a range of assumptions to reduce the number of parameters characterizing the network geometry: (1) normal pore-body and pore-throat size distributions, (2) the mean pore-body size as twice the mean pore-throat size, (3) equal relative standard deviations for the pore throats and bodies, (4) nonoverlapping pore-body and throat size distributions, and (5) strong spatial correlations among pore-throat and pore-body sizes. The lattice constant is given by $\lambda=[(1-Z/2)/\chi_v]^{1/3}$, because we require the network to possess the same Euler number per volume χ_v, as the sphere packing.

The assumptions above leave us with two calibration parameters: the coordination number Z and the nondimensional mean pore-body radius $\overline{r_b}/\lambda$, which solely determines the pore-size distributions. We determine Z and $\overline{r_b}$ by minimizing the quadratic error between $F(r)$ of the digital porous medium and the pore network using a constrained optimization algorithm [36].

3. Effective-medium approximation

For pore networks, the effective-medium approximation (EMA) can be used to estimate κ without solving any flow equations. The EMA substitutes the heterogeneous network with a uniform one, where all pore connections possess the same effective conductance g_e, which satisfies the integral equation

$$\int_0^\infty N(g)\,\frac{g-g_e}{g+g_e(Z_0/2-1)}\,dg=0, \tag{2.4}$$

where $N(g)$ is the distribution function of the pore connection conductances g [37]. Note that $N(g)$ represents also the pore throats, which have been cut ($g=0$) to achieve networks with $Z<Z_0$. The permeability is then given by $\kappa=g_e\eta/\lambda$.

III. NUMERICAL RESULTS

A. Porous media

We simulated 25 different sphere packings using the computer code developed by Yang, Miller, and Turcoliver [27]. The sphere packings had log-normal grain-size distributions, for which $\overline{D}_2=\overline{D}[1+(\sigma_D/\overline{D})^2]^2$. To achieve reliable packings, we simulated packings with at least 10 000 spheres. The packings were statistically described by $\overline{D}$, σ_D, and ϕ. We did not prescribe spatial correlations for the sphere sizes. The porosity ϕ ranged from 0.33 to 0.45 and the relative standard deviation of the grain size, $\tilde{\sigma}_D=\sigma_D/\overline{D}$, from 0 to 0.66.

TABLE I. Sphere-packing realizations for the RSP1 and RSP23 porous media.

	RSP1	RSP23
$\overline{D}$ (mm)	0.199 96± 0.0011	0.192 46± 0.1245
L (mm)	4.250	6.192
ϕ	0.442	0.334
N_g	103 28	143 80

To estimate the error in κ caused by a finite discretization and domain size, we thoroughly investigated two of the 25 packings, the most uniform (RSP1) with $\tilde{\sigma}_D=0.005$ and the least uniform (RSP23) with $\tilde{\sigma}_D=0.65$. Table I lists the properties of these packings, where L is the domain length and N_g the number of spheres.

B. LB modeling

1. Discretization effects

We simulated low Reynolds number flow ($\mathrm{Re}<1$) through the RSP1 and RSP23 packings and varied the number of voxels m along each dimension of the cubic domain. Let κ_m denote the permeability obtained at discretization m. κ_m converges to κ_∞ as $m\to\infty$. We considered a level m to provide a discretization-independent κ if $|\kappa_m-\kappa_\infty|/\kappa_\infty<0.5\%$.

We used Richardson's extrapolation to estimate κ_∞ by assuming that $\kappa_m-\kappa_\infty\sim(1/m)^n$, where n is the order of the numerical convergence. We then estimated κ_∞ from the simulations at level m_1 and a finer level m_2:

$$\kappa_\infty\approx\frac{(m_2/m_1)^n\kappa_{m_2}-\kappa_{m_1}}{(m_2/m_1)^n-1}. \tag{3.1}$$

From the results in Table II, we determined $n=2.02$ for the RSP1 and $n=2.05$ for the RSP23 packing. Those values reveal that second-order convergence can be achieved, not only for flow in simple geometries, but also for flow in porous media, consistent with the observation of Maier *et al.* [29]. Based on κ_{256} and κ_{512}, we calculated $\kappa_\infty=6.311\times10^{-7}\,\mathrm{cm}^2$ for RSP1 and $\kappa_\infty=8.082\times10^{-8}\,\mathrm{cm}^2$ for RSP23. For both packings, κ becomes discretization independent if $m\geqslant256$. Expressed in terms of the number of lattice nodes per mean sphere diameter ζ, this condition becomes $\zeta>12$, as shown in Fig. 4.

This result differs from the investigation of Maier *et al.* [29], who obtained $\zeta=36.6$ for a packing of 222 uniform spheres. They observed 30% error compared with κ_∞ at the same discretization level at which we reached resolution-independent results. This is likely due to the fact that they used $\tau=1$.

To verify our findings, we considered a subset of the RSP1 packing containing 262 spheres labeled as RSP1-sub.

TABLE II. Results of the investigation on the dependence of the permeability κ on the discretization level m for $\tau=0.8$.

Medium	m	ζ	Re	u_d'	ϕ	κ (cm^2)
RSP1	64	3.0	0.04	1.287×10^{-4}	0.443	9.190×10^{-7}
RSP1	128	6.0	0.02	4.635×10^{-5}	0.442	6.890×10^{-7}
RSP1	256	12.0	0.02	2.100×10^{-5}	0.442	6.321×10^{-7}
RSP1	512	24.0	0.09	4.195×10^{-5}	0.442	6.314×10^{-7}
RSP1-sub	32	5.1	0.14	2.743×10^{-3}	0.441	7.145×10^{-7}
RSP1-sub	64	10.2	0.51	4.899×10^{-3}	0.441	6.379×10^{-7}
RSP1-sub	128	20.4	0.42	2.067×10^{-3}	0.442	6.393×10^{-7}
RSP1-sub	256	40.9	0.41	9.970×10^{-4}	0.442	6.410×10^{-7}
RSP1-sub	512	81.8	0.06	7.877×10^{-5}	0.442	6.410×10^{-7}
RSP23	64	2.9	0.15	3.758×10^{-4}	0.334	12.01×10^{-7}
RSP23	128	5.7	0.04	5.520×10^{-4}	0.334	8.818×10^{-7}
RSP23	256	11.4	0.04	2.123×10^{-4}	0.334	8.047×10^{-7}
RSP23	512	22.8	0.03	1.019×10^{-4}	0.334	8.073×10^{-7}

We then performed the same discretization effect investigations. As shown in Table II and Fig. 4, we obtained a discretization-independent κ at the same ζ value as for the RSP1 packing, which supports our previous conclusion. Once again, we tried $\tau=1$ and obtained 19% error at this ζ value.

2. REV

We studied the impact of the domain size L on κ due to the pore-space's randomness. We used the digital representations of the RSP1 and RSP23 packings with 256^3 voxels, which yielded a resolution-independent κ. We cut both digital pore spaces into nonoverlapping cubic equal-sized subdomains. We obtained 8 subdomains with 128^3 voxels, 64 with 64^3, and 512 with 32^3, then simulated low Reynolds number flow (Re$\leqslant$0.04) in each of the subdomains.

Figure 5 shows the arithmetic mean and the standard deviation σ_κ of κ versus the nondimensional domain size $L/\overline{D}$. We considered a domain to be a REV, if $\sigma_\kappa/\kappa_{\rm tot}<5\%$, where $\kappa_{\rm tot}$ is the permeability of the entire domain. We obtained an REV for the RSP1 packing if $L/\overline{D}\geqslant10.6$, and for the RSP23 packing if $L/\overline{D}\geqslant16.1$. These values are larger than those of Bosl, Dvorkin, and Nur [16], who found $L/\overline{D}\geqslant2$ for a packing of uniform spheres (similar to our RSP1 packing). We believe our value is more accurate, because we considered multiple realizations for the pore spaces.

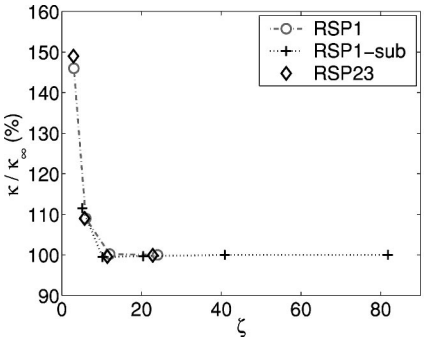

FIG. 4. Ratio of the permeability κ to κ_∞ versus the number of lattice nodes per mean sphere diameter ζ, for three porous media, simulated by LB methods.

3. Reynolds number effects

We simulated flow in the RSP1 and RSP23 packings for Reynolds numbers Re up to 25 to determine Re_0, below which Eq. (1.1) leads to faithful predictions of κ. For the uniform RSP1 packing, κ computed by Eq. (1.1) decreases by less than 1% from Re$\approx$0 to Re=5; then the error increases to 19% for Re=22. Our results are consistent with those of Maier *et al.* [29], who reported a nearly constant κ in a uniform sphere packing for Re$\leqslant$3. For the more heterogeneous RSP23 packing, inertia becomes important earlier—at Re$\approx$1.

In reality, κ does not depend on Re, rather, Eq. (1.1) loses its validity for increasing Re. We fitted our data to Ergun's equation (1.5), which describes flow for Re$>\mathrm{Re}_0$. We obtained $A=176$ for the RSP1 and $A=155$ for the RSP23 packing, assuming $B=0$ for Re$<$5 for RSP1 and Re$<$1 for RSP23. As Re increases, inertial forces represented by the B term in Eq. (1.5) gain importance. By fitting the data for

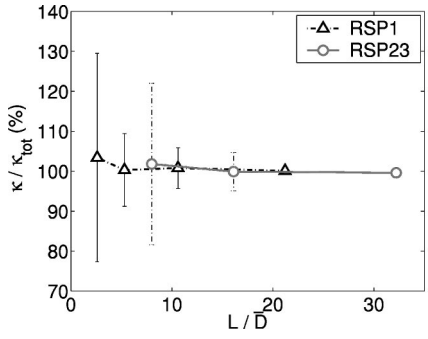

FIG. 5. Permeability κ, normalized by the permeability of the entire domain $\kappa_{\rm tot}$, versus domain size $L/\overline{D}$ for the RSP1 and RSP23 packings, simulated by LB methods. The length of the error bars stands for twice the standard deviation due to the pore-space's randomness.

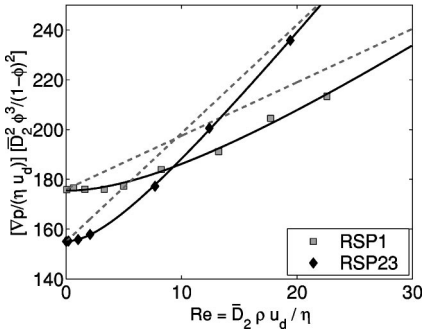

FIG. 6. Our model (solid lines) for the relation between the nondimensional pressure drop and the Reynolds number agrees well with our simulations (symbols) and also describes the Darcian flow regime as opposed to Ergun's equation (dashed lines).

larger Re, we determined $B=1.2$ for the RSP1 and $B=2.9$ for the RSP23 packing. Our results for A and B agree well with the empirical values by MacDonald *et al.* [10].

Equation (1.5) however, does not describe the nearby constant drop in nondimensional pressure for $\mathrm{Re} \ll \mathrm{Re}_0$ in the Darcian flow regime. Therefore, we suggest

$$\frac{\nabla p}{\eta u_d} \frac{\overline{D_2^2}\phi^3}{(1-\phi)^2} = A' + B' \frac{\mathrm{Re}}{\mathrm{Re}+\mathrm{Re}_0} \frac{\mathrm{Re}}{1-\phi}, \tag{3.2}$$

where A', B', and Re_0 are fit parameters that depend on the pore geometry. Note that this relation unambiguously defines Re_0. Figure 6 shows a good agreement between our new correlation, given by Eq. (3.2), and the simulated data in both the Darcian and non-Darcian regime for both the RSP1 and RSP23 packing. Table III shows the fit parameters. Relating A', B', and Re_0 to the porous medium properties would have required simulations in more media and was beyond the scope of this paper.

4. Correlation model for permeability

From the studies in our most nonuniform packing with $\tilde{\sigma}_D=0.66$, we found that the error due to finite discretization was smaller than 0.5%, if $\zeta>12$, and the error due to finite domain size was smaller than 5% if $L/\overline{D}>16$. Based on this information, we chose subsets of the 25 sphere packings and digitized them such that these conditions were fulfilled. By dimensional analysis, the permeability of a packing is given by

$$\frac{\kappa}{\overline{D^2}} = f(\phi, \tilde{\sigma}_D). \tag{3.3}$$

TABLE III. Fit parameters for our model for the relation between the nondimensional pressure drop and Re.

	RSP1	RSP23
A'	175.50	155.12
B'	1.83	3.81
Re_0	36.73	10.89

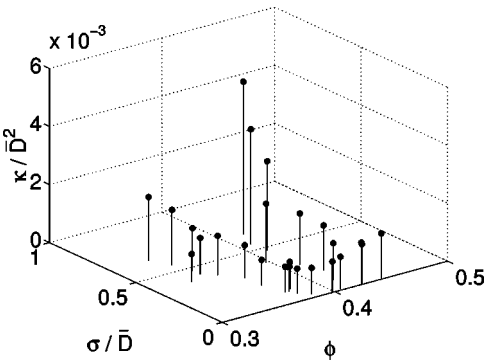

FIG. 7. Permeability κ obtained by LB modeling versus the porosity ϕ and relative standard deviation $\tilde{\sigma}_D$ of the sphere diameter.

Figure 7 shows the simulated $\kappa/\overline{D^2}$ versus ϕ and $\tilde{\sigma}_D$.

We compared our simulation results to both the Carman-Kozeny and the Rumpf-Gupte relations. The latter is based upon experiments in random sphere packings, one with a narrow sphere-size distribution $\tilde{\sigma}_D=0.0945$, and two with broader distributions $\tilde{\sigma}_D=0.320$ and 0.327. The porosities ϕ ranged from 0.35 to 0.7. Figure 8 shows how well our simulated values agree with measured κ values within the ϕ and $\tilde{\sigma}_D$ ranges of Rumpf and Gupte's experiments. For media with porosities and size distributions beyond their experimentally supported ranges, however, the Rumpf-Gupte relation deviates significantly from our results. Figure 8 also suggests that the Carman-Kozeny relation underpredicts κ of sphere packings, because both the empirical Rumpf-Gupte relation and our simulations yield larger κ values. For lower porosities, the Carman-Kozeny relation deviates significantly from our simulation results. This finding is consistent with [6,7].

We fitted our simulation results to a correlation model derived from the Rumpf-Gupte relation (1.4):

$$\frac{\kappa}{\overline{D_2^2}} = \beta_1 \phi^{B_2}, \tag{3.4}$$

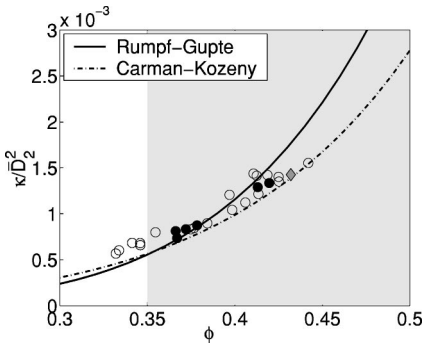

FIG. 8. Comparison between LB simulations and empirical relations. Solid circles indicate packings with $0.1<\tilde{\sigma}_D<0.33$. The gray area marks those porosities, which are supported experimentally by Rumpf and Gupte. The diamond stands for an LB simulation performed by Maier *et al.* in a uniform sphere packing.

TABLE IV. Fit parameters of the permeability function (3.5) including 95% confidence intervals.

β_1	0.0397 ± 0.0058
β_2	3.9513 ± 0.1610
β_3	8.3000 ± 0.5215
β_4	2.2335 ± 0.1249

where β_1 and β_2 are fit parameters. We used the Gauss-Newton algorithm to minimize the sum of the quadratic differences between simulated and fitted κ values. The fit results, however, were not optimal. By expressing the correlation in terms of $\overline{D}$ and $\tilde{\sigma}_D$—as suggested by Eq. (3.3)—and not only in terms of $\overline{D}_2$, we achieved much better results. Like Rumpf and Gupte, we assumed that the right-hand side of Eq. (3.3) can be separated with respect to ϕ and the remaining fit parameters. We posited

$$\frac{\kappa}{\overline{D}^2} = \beta_1 \phi^{\beta_2}(1+\beta_3 \tilde{\sigma}_D^{\beta_4}), \tag{3.5}$$

with four fit parameters. The sum of quadratic differences between the simulated and fitted κ values based on our new correlation was ten times less than on Eq. (3.4). Table IV lists the fitted parameters, and Fig. 9 compares the correlation model to our simulated data.

C. Pore-network modeling

1. Calibration

We performed flow simulations in pore networks for the RSP1 and RSP23 packings. For calibrating the pore-network models, we determined the morphological pore-size distributions of the sphere packings, shown in Fig. 10, and the specific Euler number χ_v, shown in Table V. Table V also shows the properties of the calibrated networks.

2. REV

Because of the pore network's randomness, the network size L has an effect on κ. Similar to LB modeling, we studied this effect by generating cubic networks with 64 pore bodies along every direction for the RSP1 and RSP23 packings. We subdivided these networks into 8 subdomains with 32^3 pore bodies, 64 with 16^3, 512 with 8^3, and 4096 with 4^3, then simulated flow in each of the networks. Then, we obtained the mean and standard deviation of the simulated κ for equal-sized subdomains.

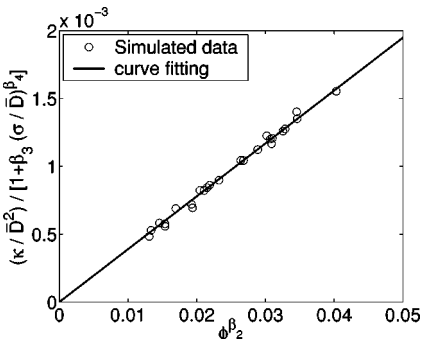

FIG. 9. Our correlation model for the permeability of sphere packings describes LB modeling results accurately.

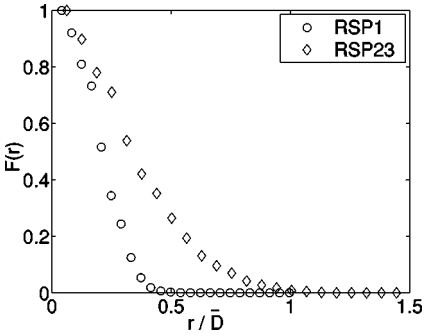

FIG. 10. Morphological pore-size distribution $F(r)$ of the RSP1 and RSP23 packings.

Using the same criteria as for LB modeling, networks with at least 8^3 pore bodies yield a REV. Figure 11 shows that $L/\overline{D} \geqslant 6.7$ yields a REV for the RSP1, $L/\overline{D} \geqslant 10.4$ for RSP23 packing, which is about 40% less than the REV obtained by LB modeling. We expected disagreement between both pore-scale modeling approaches, because a pore-network model does not represent all aspects of the sphere-packing's morphology, such as the shape of the pore space and spatial correlations.

3. Absolute permeability values

We compared the pore-network modeling results with κ_∞ from LB modeling. Assuming that LB modeling faithfully predicts κ, Fig. 11 shows that the pore-network model underestimates κ by up to 40%. Nonetheless, our pore-network calibration approach still yields an acceptable prediction for κ when compared to other approaches: (1) Fischer and Celia [20], who calibrated their network by matching simulated and measured capillary pressure-saturation curves, obtained similar errors; (2) Vogel and Roth [23], who calibrated their network by mapping a three-dimensional representation of a pore space onto a pore-throat network, simulated permeabilities which differed by an order of magnitude from experimental values.

We also compared the simulated κ with the predictions from the EMA. Figure 11 shows deviations smaller than 5% for both packings. This agreement was obtained, because the calibrated networks are well above the percolation threshold, with $Z=5.9$ for the RSP1 and $Z=6.0$ for the RSP23 packing.

TABLE V. Calibration results.

	RSP1	RSP23
χ_v (mm^{-3})	-407	-128
Z	5.9	6.0
$\overline{r_b}\lambda$	0.3395	0.3130

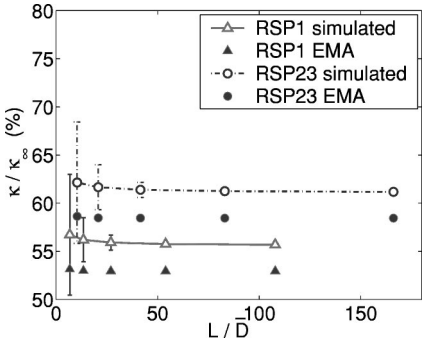

FIG. 11. Permeability κ obtained by pore-network modeling normalized by κ_∞ from LB modeling versus the nondimensional domain length $L/\overline{D}$. The length of the error bar stands for twice the standard deviation of κ due to the pore-space's randomness.

IV. DISCUSSION AND CONCLUSIONS

(1) The LB modeling of laminar duct flow agrees well with the analytical solution. Furthermore, we obtain good agreement between LB simulations and the empirical Rumpf-Gupte relation for the permeability κ of sphere packings for those porosity values that are experimentally supported. LB modeling also agrees well with the Ergun equation for higher Reynolds number flow. We conclude that LB modeling faithfully describes the flow process and that our simulated sphere packings represent the experimental sphere packings well.

(2) The relaxation time τ has an essential impact on the accuracy achieved. Although $\tau=0.8$ requires more iterations to achieve convergence than $\tau=1.0$, the results are more accurate. This is important in particular for LB simulations, where memory limitations often do not allow a fine discretization.

(3) We find that the Carman-Kozeny relation underestimates the κ of sphere packings. We also observe deviations between LB modeling and the empirical Rumpf-Gupte relation for those porosity values lacking experimental support. Using LB simulations, we suggest a correlation model for κ of sphere packings with log-normal sphere-size distribution. This model allows an estimation of κ in terms of the porosity, and the mean and standard deviation of the sphere diameter. These quantities lead to a better fitting of our results than the surface mean diameter and porosity alone.

(4) Compared with LB modeling, which presumably predicts κ faithfully, pore-network modeling underestimates κ by up to 40% due to a loss of information when mapping the sphere packing onto the pore-network geometry. This underestimation is consistent with the fact that κ increases with the pore-space's correlation length [38], because our network calibration does not account for spatial correlations of the pore size, which intrinsically exist in sphere packings. Nevertheless, our calibration approach still predicts κ well compared to other published calibration approaches.

(5) An LB approach is computationally much more demanding than a pore-network approach because of memory and CPU time requirements. Simulating flow in a REV of the RSP1 packing, for example, required 20 total CPU hours on an IBM-SP2 using LB modeling and 128 processors as opposed to a few seconds on a SGI Origin 2000 using network modeling and one processor. For these simulations, the size of the numerical domain corresponded to 8^3 pore bodies for pore network modeling and 1200 spheres discretized by 128^3 voxels for LB modeling. Our pore-network modeling approach, however, needs a morphological analysis of the sphere packing, which currently requires several days CPU time on a SGI Origin 2000 using one processor.

ACKNOWLEDGMENTS

This work was supported by National Science Foundation (NSF) Grant No. EAR-9901660, National Institute of Environmental Health Science (NIEHS) Grant No. 5 P42 ES05948-02, and a URC grant from the University of North Carolina. We also would like to thank the North Carolina Super Computing Center (NCSC) for supercomputing time and Marc Reed (NCSC) for useful discussions and assistance with optimizing of our codes.

[1] M. A. Celia, P. C. Reeves, and L. C. Ferrand, Rev. Geophys. **33**, 1049 (1995).
[2] F. A. L. Dullien, *Porous Media: Fluid Transport and Pore Structure* (Academic, San Diego, CA, 1992).
[3] P. Z. Carman, *Flow of Gases Through Porous Media* (Butterworths, London, 1956).
[4] R. B. Bird, W. E. Stewart, and E. N. Lightfoot, *Transport Phenomena* (Wiley, New York, NY, 1960).
[5] H. Rumpf and A. R. Gupte, Chemie Ingenieur Technik **43**, 367 (1971).
[6] N. S. Martys, S. Torquato, and D. P. Bentz, Phys. Rev. E **50**, 403 (1994).
[7] L. M. Schwartz, N. Martys, D. P. Bentz, E. J. Garboczi, and S. Torquato, Phys. Rev. E **48**, 4584 (1993).
[8] A. E. Scheidegger, *The Physics of Flow Through Porous Media* (Macmillan, New York, 1960).
[9] J. Bear, *Dynamics of Fluids in Porous Media* (Dover, New York, 1972).
[10] I. F. MacDonald, M. S. El-Sayed, K. Mow, and F. A. L. Dullien, Ind. Eng. Chem. Fundam. **18**, 199 (1979).
[11] S. Chen and G. D. Doolen, Annu. Rev. Fluid Mech. **30**, 329 (1998).
[12] S. Succi, E. Foti, and F. Higuera, Europhys. Lett. **10**, 433 (1989).
[13] R. S. Maier, D. M. Kroll, Y. E. Kutsovsky, H. T. Davis, and R. S. Bernard, Phys. Fluids **10**(1), 60 (1998).
[14] S. Hou, Q. Zou, S. Chen, G. Doolen, and A. C. Cogley, J. Comput. Phys. **118**, 329 (1995).
[15] A. Koponen, M. Kataja, and J. Timonen, Phys. Rev. E **56**, 3319 (1997).
[16] W. J. Bosl, J. Dvorkin, and A. Nur, Geophys. Res. Lett. **25**(9), 1475 (1998).

[17] D. Zhang, R. Zhang, S. Chen, and W. E. Soll, Geophys. Res. Lett. **27**(8), 1195 (2000).
[18] T. Inamuro, M. Yoshino, and F. Ogino, Int. J. Numer. Methods Fluids **29**, 737 (1999).
[19] E. H. D'Hollander, Water Resour. Res. **15**, 107 (1979).
[20] U. Fischer and M. A. Celia, Water Resour. Res. **35** (4), 1089 (1999).
[21] S. L. Bryant, P. R. King, and D. W. Mellor, Transp. Porous Media **11**(1), 53 (1993).
[22] H. J. Vogel and K. Roth, Eur. J. Soil. Sci. **49** (4), 547 (1998).
[23] H. J. Vogel and K. Roth, Adv. Water Res. **24**, 233 (2001).
[24] S. Bakke and P.-E. Oren, SPE J. **2**, 136 (1997).
[25] S. Mishra, J. C. Parker, and N. Singhal, J. Hydrol. **108**, 1 (1989).
[26] L. M. Ayra and T. S. Dierolf, in *Indirect Methods for Estimating the Hydraulic Properties of Unsaturated Soils*, edited by M. Th. van Genuchten (U.S. Salinity Laboratory, Riverside, CA, 1992), pp. 115–124.
[27] A. Yang, C. T. Miller, and L. D. Turcoliver, Phys. Rev. E **53**, 1516 (1996).
[28] Q. Zou and X. He, Phys. Fluids **9**(6), 1591 (1997).
[29] R. S. Maier, D. M. Kroll, H. T. Davis, and R. S. Bernard, Int. J. Mod. Phys. C **9**(8), 1523 (1998).
[30] R. S. Maier, R. S. Bernard, and D. W. Grunau, Phys. Fluids **8**(7), 1788 (1996).
[31] D. H. Fenwick and M. J. Blunt, SPE J. **3**, 86 (1998).
[32] M. Hilpert, R. Glantz, and C. T. Miller (unpublished).
[33] R. Glantz, Porennetzwerke von Erdstoff-Filtern: Mathematisch-morphologische Beschreibung kernspintomographischer Aufnahmen., Ph.D. thesis, Universität Karlsruhe, Karlsruhe, 1997.
[34] G. Lohmann, *Volumetric Image Analysis* (Wiley, Chichester, 1998).
[35] H. Bieri and W. Nef, Comput. Vis. Graph. Image Process. **28**, 166 (1984).
[36] P. Gilmore and C. T. Kelley. IFFCO: Implicit filtering for constrained optimization. Technical Report CRSC-TR93-7, Center for Research in Scientific Computation, North Carolina State University, Raleigh, 1993.
[37] S. Kirkpatrick, Rev. Mod. Phys. **45**, 574 (1973).
[38] D. T. Hristopulos and G. Christakos, Stoch. Environ. Res. Risk Assessment **13**, 1 (1999).